NUMERICAL SIMULATION OF PLASTIC DEFORMATION PROCESSES FROM CAST IRON PARTS

Tudor CHERECHES [1], Paul LIXANDRU [1], Sergiu MAZURU [2], Pavel COSOVSCHI [3] and Daniel DRAGNEA [1]

ABSTRACT: One of the various proceedings for material cold-work hardening is the smooth finishing by superficial plastic deformation with hard tools from metallic carbide or diamond. According to this procedure, the active workpiece faces are pressed with a tool, generally ball-shaped, which has a spatial compound movement. The contact between tool and workpiece, also in motion, is force/displacement controlled. This paper describes a numerical simulation for study of the such-like procedure, used for cast iron parts. An accurate physical model for technological process was stated. The attention was focused on the material elastic-plastic properties and on constitutive equations. The finite element discretization with more fine mesh in the superficial layers of the workpiece active faces was achieved. The LS-DYNA explicit dynamic code was used for solving and analyses. The numerical simulation was applied on workpieces of revolution, manufactured by contour turning.
KEYWORDS: numerical simulation, LS-DYNA, physical model, mathematical model, numerical solution.

1 INTRODUCTION

In present days numerical simulation became an important tool of engineering. The numerical simulations follow a similar procedure to all the scientific approaches, which consist in passing through several stages. Starting from phenomenon or process, the physical model is created.

A mathematical model expresses the physical laws under quantitative shape with the aid of the governing equations. The following stage, very important for the user of this numerical procedure, is the discrete model design. In this stage, the investigator, using one of the available pre-processing codes, creates an adequate mesh or nodal grid in the problem domain. A well-chosen mesh (grid) satisfies the two antagonistic conditions: a good accuracy and reasonable computational effort.

After meshing, all problem conditions are inserted and the pre-processing is finished. In the next stage, the code solver takes over whole computational effort and gives the problem solution under numerical form.

The last stage consists in data post-processing, which has as goal the solution completing, additional computations and result analysis. Except the mathematical model, in this work were crossed all numerical simulation stages, with particular attention on the physical model configuration, especially on the material models and on the final solution analysis.

[1]SC UPS PILOT ARM SRL, Dragomiresti, 137210, România

[2]UTM FIMCM, Str. Studentilor, 9, Blocul de Studii nr. 6, MD-2045, Chisinau, Moldova Republic

[3]FABRICA DE STICLA, Chisinau, str.Transnistria nr. 20, Moldova Republic
tudor.chereches@yahoo.com; s_mazuru@mail.utm.md; c.pashag@gmail.com**;** danieldrg2003@yahoo.com

2 PHYSICAL MODEL

The configuration of the smooth finishing process physical model for workpieces of revolution, considered in present study, shown in Fig. 1a consists in: the mandrel with jaws, the tool with active part in ball-shape and workpiece.

The tool action is controlled using some fictive transducers for force measurement. The simulated working of the regime parameters are: the machine spindle speed and the longitudinal and radial advances. During off the smooth finishing process the spindle speed and, consequently, workpiece speed remain constant. The two advancing movements are correlated in order to obtain the desired profile. In all applications, the longitudinal (axial) advance is constantly kept, following that the radial advance to be adjusted according to the contact surface profile. To achieve the major goals of numerical simulation of the plastic deformation technological process, there are conceived the model bodies with three types of active surfaces: cylindrical, conical and cubic spline profiled shape, as presented in Fig. 1b.

On the active surfaces, a random roughness was generated. In physical model design, an important place is reserved for material model formulation.

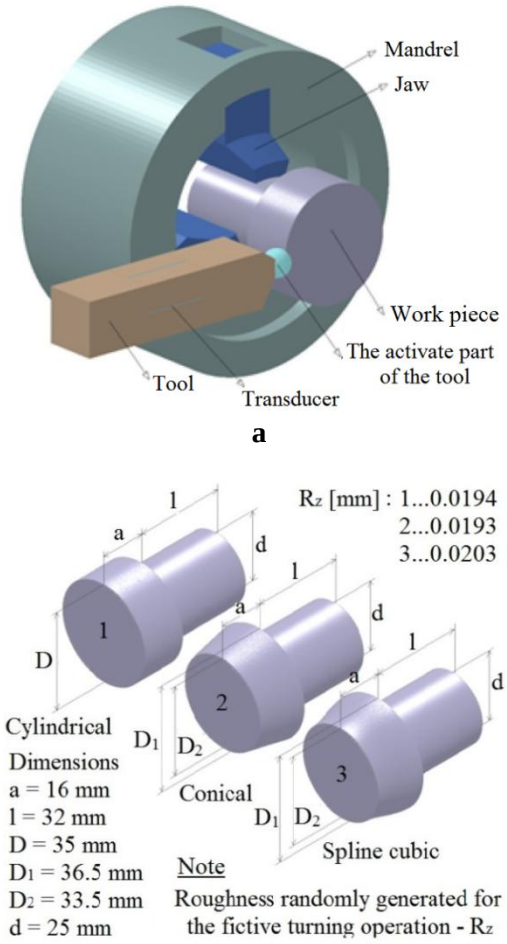

Figure 1. The physical model for the technological process of cold plastic deformation and workpiece model

3 MATERIAL MODEL

Generally, in practice, parts made of iron cast with lamellar graphite are often used. This is the study case. The plasticity of the lamellar graphite gray cast iron in stress state in which prevail tractions is very low and therefore it is necessary to avoid apparition of the tensile stress in workpieces during smooth finishing process. In the plastic deformations of metals, besides the mechanical properties, some thermal properties are involved. Basic elastic-plastic properties of the materials used in applications are distinguished through characteristic diagrams of cast iron in simple compression tests which were carried out at attested laboratories. Additionally, in the same laboratories Brinell and Vickers hardness tests were performed.

In the compression test, three lots of standard specimens, taken from different casting charges have been tried. The conversion of the raw recorded curves obtained in compression tests in real (true) characteristic diagrams, shown in Fig. 2, was

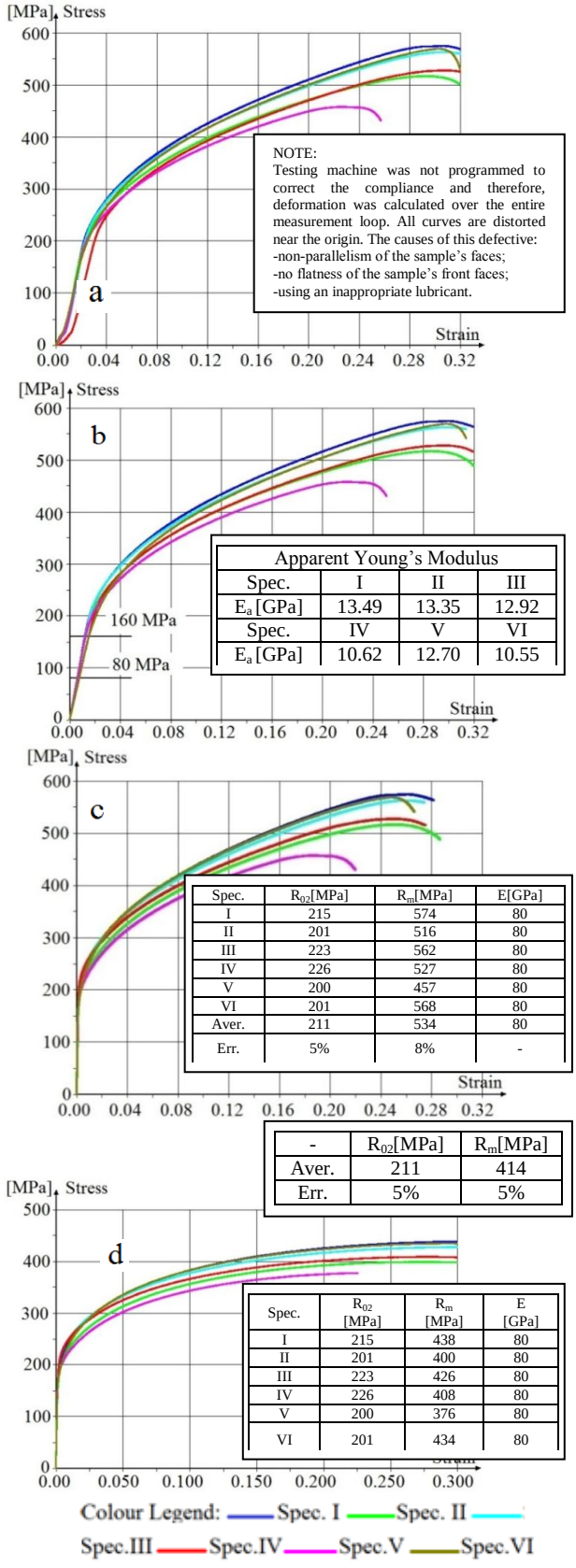

Apparent Young's Modulus

Spec.	I	II	III
E_a [GPa]	13.49	13.35	12.92
Spec.	IV	V	VI
E_a [GPa]	10.62	12.70	10.55

Spec.	R_{02}[MPa]	R_m[MPa]	E[GPa]
I	215	574	80
II	201	516	80
III	223	562	80
IV	226	527	80
V	200	457	80
VI	201	568	80
Aver.	211	534	80
Err.	5%	8%	-

-	R_{02}[MPa]	R_m[MPa]
Aver.	211	414
Err.	5%	5%

Spec.	R_{02} [MPa]	R_m [MPa]	E [GPa]
I	215	438	80
II	201	400	80
III	223	426	80
IV	226	408	80
V	200	376	80
VI	201	434	80

Figure 2. Compresion characteristics diagrams for lot no. 1 a) recorded curves in raw form; b) recorded curves repaired in origin; c) conventional characteristic diagrams; d) real characteristic diagrams

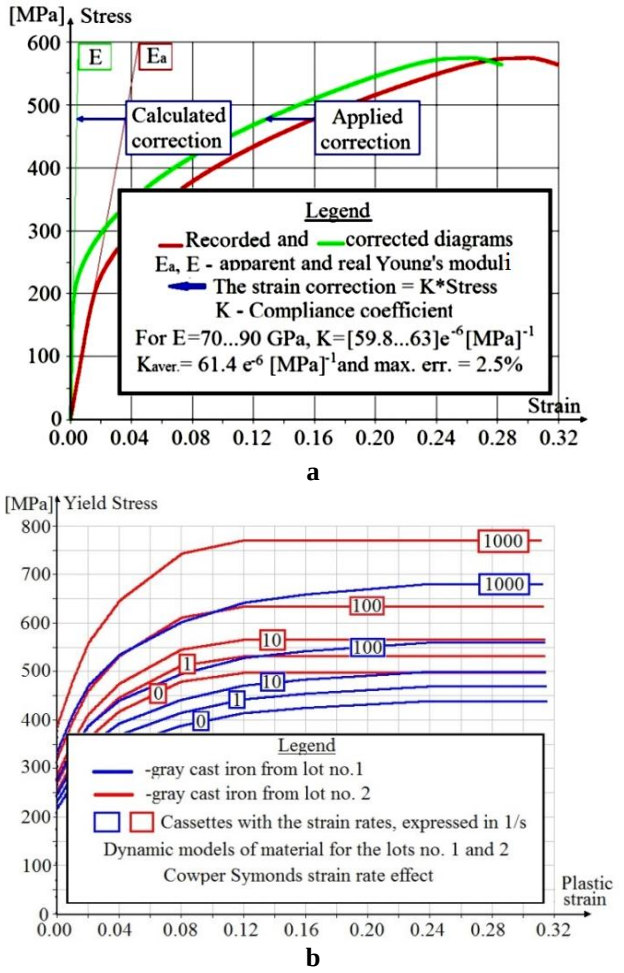

Figure 3. Compliance correction and viscosity effect; a) Compliance correction, b) Viscosity effect

achieved using a special procedure which has some steps. The raw curves conditioning are based on the assumption of the testing machine compliance linearity and was made according to Fig. 3a.

The conventional curves were transformed in real characteristic diagrams changing the engineering stress in true stress and the strain in logarithmic strain.

From space economy reasons, the experimental compression data exhibition of the lot no. 1 was exposed, only, but the real mechanical properties are completely given in the Table 1.

The value dispersion of the experimental data varies from lot by lot and even from one sample to another in the same lot, in wide limits, expressed in last column of Table 1. In this work are used averaged values on a lot.

The numerical simulations of the smooth finishing processes by plastic deformation on the workpieces employ several typical material elasto-visco-plastic models, which are below formulated and expressed by their own constitutive equations.

Table 1. Mechanical characteristics

Specimen		1	2	3	4
Yield Stress [MPa]	Lot				
	1	215	210	223	226
	2	225	210	235	255
	3	215	215	230	235
Ultimate Stress [MPa]	1	438	400	426	408
	2	425	420	404	432
	3	370	396	458	475
Brinell Hardness [HB]	1	115	107	119	125
	2	150	139	137	141
	3	126	102	112	124

Specimen		5	6	Aver.	Err. [%]
Yield Stress [MPa]	Lot				
	1	200	201	212	4.7
	2	222	215	227	6.5
	3	190	210	216	9.0
Ultimate Stress [MPa]	1	376	434	414	5.2
	2	439	424	424	2.6
	3	338	422	410	11.6
Brinell Hardness [HB]	1	110	137	118	8.7
	2	138	136	140	3.7
	3	115	119	116	6.9

4. CONSTITUTIVE EQUATIONS

In the plasticity, stated on plastic flow theory, the main constitutive equations have an incremental form (Khachanov, 1974) and express proportionality between the increments of plastic strain, $d\varepsilon_{ij}$, and components of stress deviator, s_{ij}, $d\lambda$ being an infinitesimal factor (Eq. 1). These equations have in plasticity the same importance as Hooke's law in elasticity.

$$d\varepsilon_{i,j}^{p} = d\lambda s_{i,j} \,. \tag{1}$$

Additionally, the plasticity constitutive equations contain a connection which expresses the dependence of the yield stress on the material state, plastic strain, plastic strain rate and temperature. The yield stress equation models the material response in action and is exclusively based on experimental data, obtained from static and dynamic testes, at normal, low and high temperatures. The plastic stress-strain curves are obtained from real characteristic curves (Fig. 2d) eliminating the elastic component of strain. In this case, the plastic characteristic curve begins with initial yielding stress (Fig. 3b). In numerical simulations performed in this work a most popular schematization exponentially expressed by binomial equation was used,

$$\sigma_y = A + B\varepsilon_p^n \,, \tag{2}$$

where σ_y is the yielding stress, ε_p - effective plastic strain and A, B and n are material constants

which are obtained based on the minimum errors. For n=1 linear plastic with or without hardening model results. The additional constitutive equation for material of the lot no. 1 was written in both forms, linear and exponential, with the coefficients given in the Table 1. For comparison, beside parameters *A*, *B* and *n*, in last column, the quadratic errors in band of effective plastic strain from 0 up to 0.32 are presented. Many complex plastic models integrate the exponential representation of the material behavior. One of them is the Johnson-Cook material model [2] which, additionally, takes into account, the strain rate and thermal effects and is expressed by the equation

$$\sigma_y = \left(A + B\varepsilon_p^n\right)x \left(1 + \ln \dot{\varepsilon}_p\right)\left[1 - \left(\frac{T - T_{r\,m}}{T_{melt} - T_{r\,m}}\right)^m\right], \quad (3)$$

where, beside Eq. 2, new terms appear. C is a coefficient, m - thermal exponent, T – local material temperature and $\dot{\varepsilon}_p$ is relative effective plastic strain rate. In this stage, in work, a simplified Johnson-Cook without thermal effect was used. As an example, for the lot no. 1 were used the following parameters: *A*=210 [MPa], *B*=660 [MPa], *n*=0.58 and *C*=0.055.

Other possibility to take in account the viscosity effect is to use the Cowper-Symond multiplier.

Using the Johnson-Cook date, *C* and *n* were approximate: *C*=7100 s^{-1} *p*=3.32. The viscous-plastic model for first two material lots used in simulations, shown in Fig, 3b, is obtained by the combination of the piecewise linear plasticity with Cowper-Symond multiplier. The viscosity effect, taken in account with the Cowper-Symond multiplier is shown in Fig. 3b for different effective plastic strain rate. The selection of the best material models was made by the comparison of Brinell test simulation results with experimental data. In Fig. 4 there are given the partial model of the simulation and effective plastic strain fields in remanent stage for both used materials. For Johnson-Cook materials model the values of Brinell simulated hardness (122 and 140) are comparable with the experimental data values (118 and 140) averaged on each material lot (Table 2). This method for material model validation is very proper, especially in the predominant compressive plastic deformations. The Johnson-Cook model is used in following simulations.

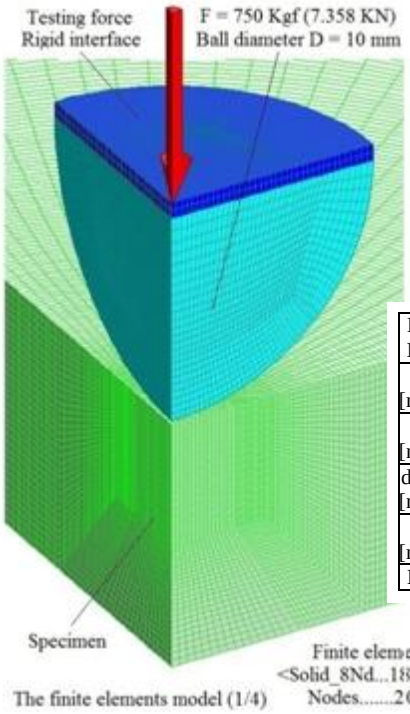

Lot No.	1	2
d_1 [mm]	5.380	4.920
d_2 [mm]	5.382	4.922
$d_{aver.}$ [mm]	5.381	4.921
h [mm]	0.737	0.627
HB	122	140

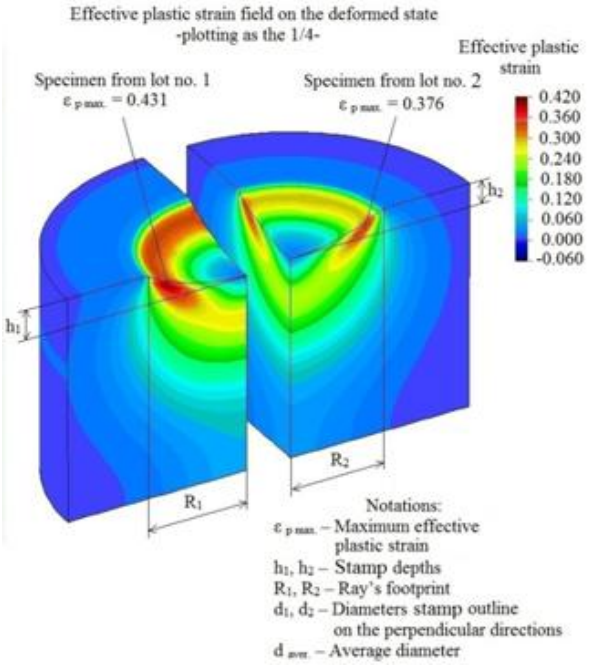

Figure 4. Brinell simulation test

5. SIMULATION

The finite element discretization of the physical model (Fig. 1) was performed with the variable density mesh by using 3D-hexaedral elements.

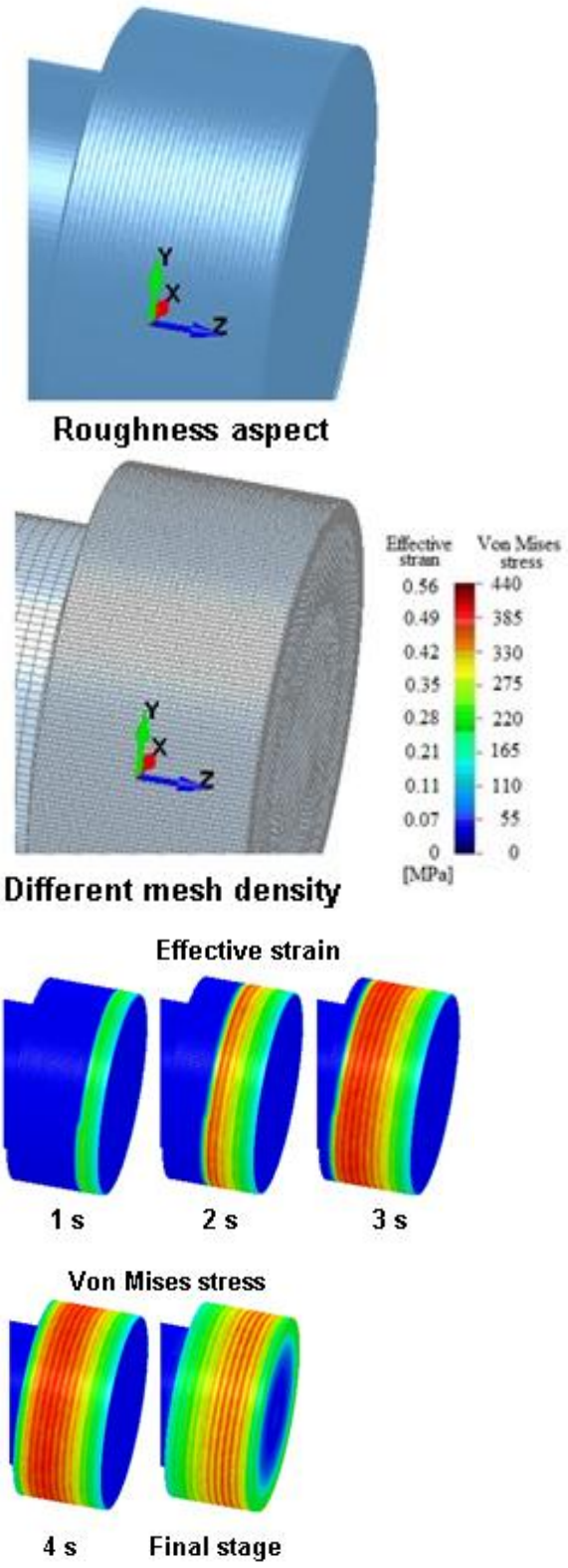

Figure 5. The workpiece discretization, effective plastic strain field and von Mises stress on active surface

The superficial layer of the workpiece was meshed with high density (Fig. 5).

The various simulation work regimes were established within of the following parameter limits: the spindle speed: 384…920 rpm; the longitudinal advance: 0.09…0.32 mm/rev; the depth: 0.05…0.2 mm. The random roughness was established in according with the middle turning operation (Ra= 3.2…6.3 μm). For each established regime, the input data were introduced in the LS-DYNA command, file and then the LS-DYNA solver was started. The complete solution is obtained. The result analysis accentuates the importance of the numerical simulation on the smooth finishing process. The surface quality may be interpret on the effective plastic strain field as that shown in Fig. 5 The field homogeneity and intensity indicate an improvement of the surface quality by hardening. By an especial procedure, using nodal coordinate in final stage, the surface roughness is evaluate. The residual stress field, represented in the same figure, relieves one of the disadvantages of this processing. The contact forces, as time functions, are shown in Fig. 6. The final plastic strain field (Fig. 5) and force variations (Fig. 6) reveals that a better control on the radial advance, for deformation uniformity, is necessary.

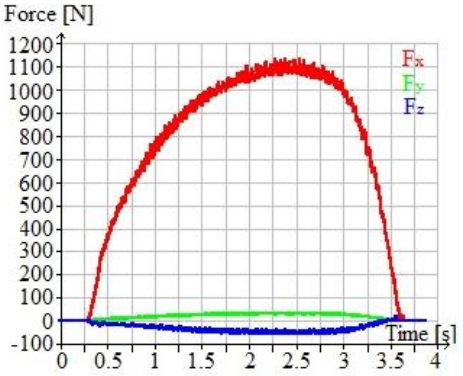

Figure 6. Simulated contact forces

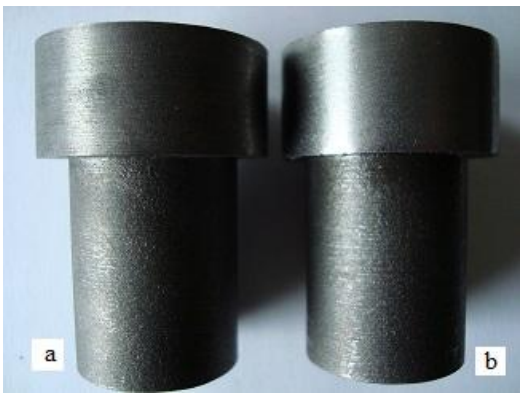

Figure 7. Workpieces a) before and b) after real smooth finishing

Fig. 8 enables qualitative analysis of machined surface depending on radial pressure force. It's a visible difference in quality, assessed by roughness of machined surfaces. In the simulation case of a radial force of 250 N, the tool failed to produce

smoothing and reduce roughness to acceptable values.

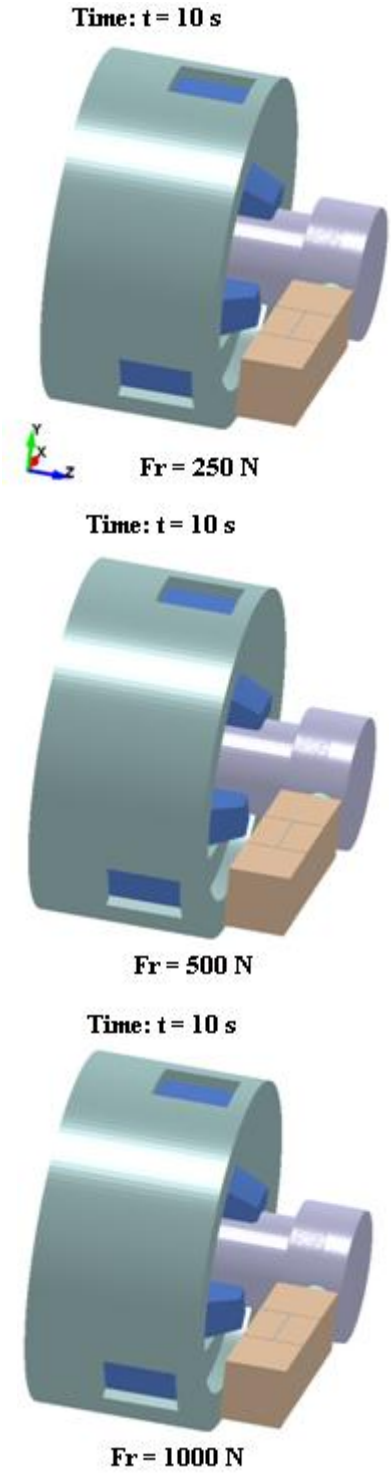

Figure 8. Qualitative analysis of machined surface depending on radial pressure force

Machining under radial force of 500 N gives a smooth surface with low roughness. Machining with larger force of 1000 N, greatly reduce roughness but produces larger deviations form by corrugations.

The above interpretation is supported by the appearance of the machined surface of Fig. 9, which is the profile of the machined surface depending on the radial force. Workpiece surface profile was represented by one of its generators in the *yoz* plane. The surface of the workpiece is divided into two parts. In front of attack's frontline of the spherical body of the tool, in the left side is found the initial portion which presents roughness randomly generated with mentioned values on the figure. Behind of the attack's frontline, the machined surface, smoothed to a certain level is found. To highlight workpiece surface profile, radial dimension is multiplied 10 times.

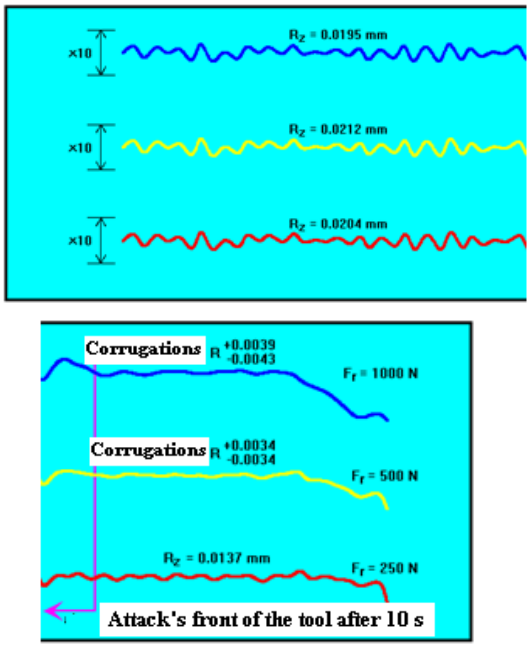

Figure 9. Machined surface profile depending on radial force

The data obtained by numerical simulation shows that the processing of the baseline data in the radial force of 250 N is not effective. Remaining roughness exceeds half from the initial one. A better smoothing with a pressing force on the tool of 500 N was performed. It is found that on the machined surface, with some periodicity, corrugations occur. These corrugations give a deviation form which, relative to the average radius is between -3.4 and +3.4 μm. Largest corrugations occur when the push force increases. Selection of the working regime of radial force in the smoothing process and hardening of the parts made of cast iron with lamellar graphite is made depending on the purpose and the initial state of the surfaces. For smoothing process of the surfaces with low roughness, on the spherical head of the tool smaller

forces are applied. When the surface roughness increases it's necessary to increase the pressing force.

In the Fig. 10, the effective remanent stress field in the machined zone after 10 s is presented. Remanent stresses intensity depends directly on the size of the radial forces applied.

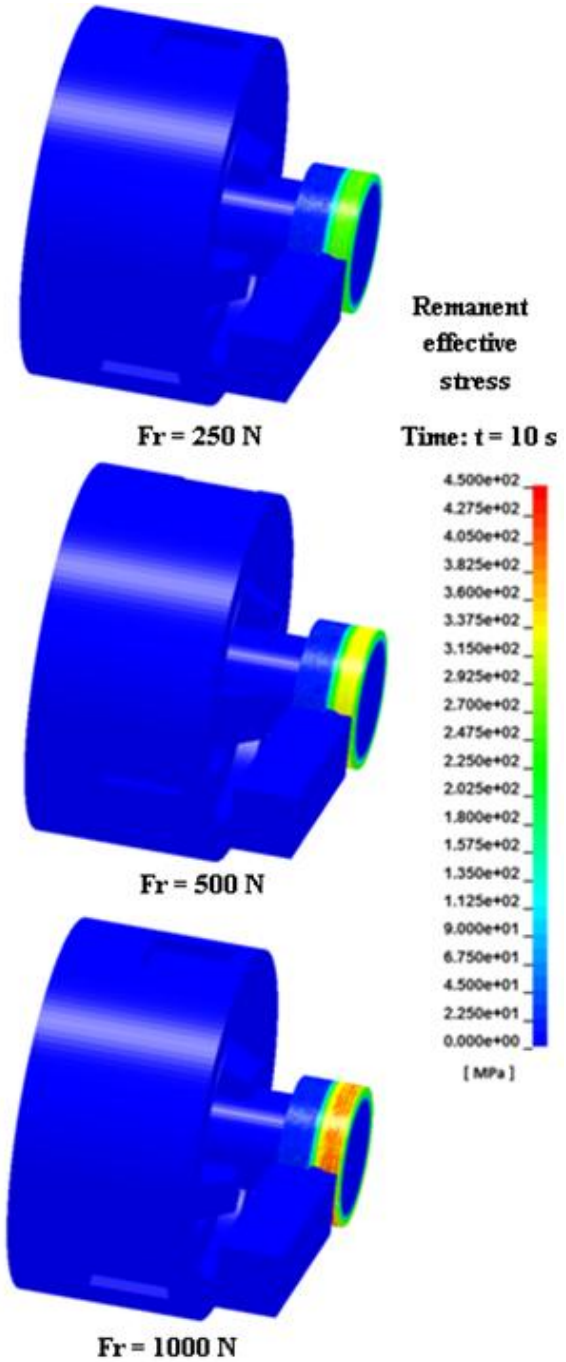

Figure 10. Remanent effective stress in the machined area after 10 s

tool, whose shape continuously changes. On the three representations, a certain periodicity of field

In homogeneity of the remanent stress fields is justified by material wave existence in front of the spherical head of the variation can be seen. It can be seen that the in homogeneity of the effective stress field depends on the force.

The result of numerical simulation of the process of smoothing and hardening by displacement control is shown in Fig. 11 in the form of effective plastic strain field. Analysis of the representations in Fig. 12 highlights the high quality of the surfaces machined by this method, compared with those obtained by the controlled force.

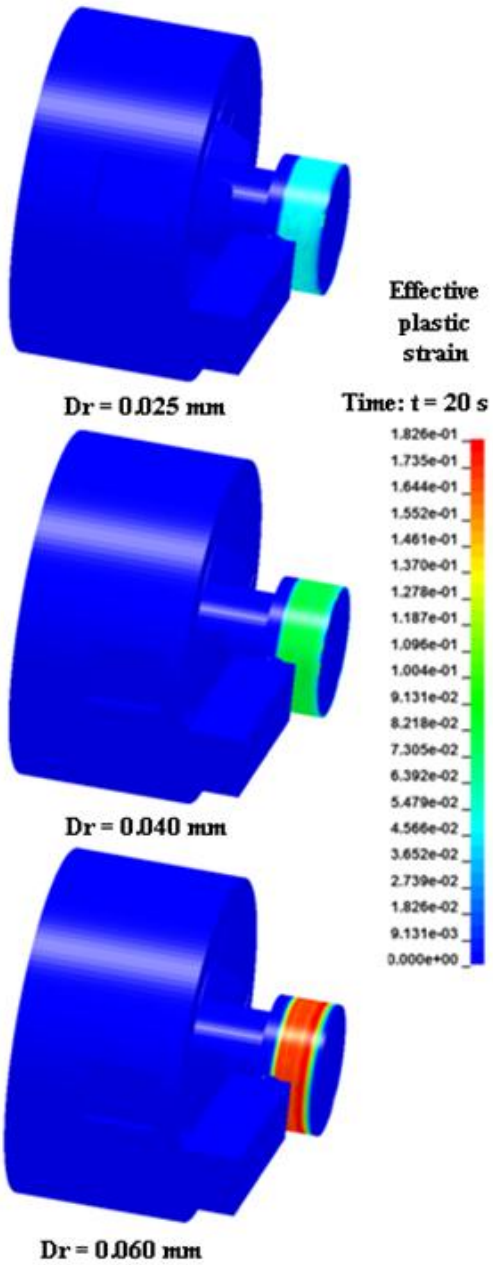

Figure 11. Effective plastic strain field at t = 20

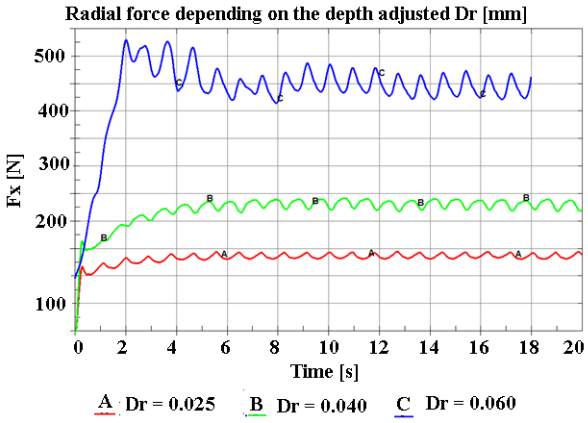

Figure 12. The radial force depending to the set depth Dr [mm]

6. CONCLUSIONS

In the work, a numerical simulation methodology for the smooth finishing processing of the glass mold tools, based on the LS-DYNA finite element codes, was formulated. An especial attention was conferred to model preparation, because if the physical model is not correctly and completely designed, neither finite element code thoroughness, nor computer capabilities vouch for solutions accuracy and numerical simulation success. This is an argument of the large space assigned in the work to material tests and constitutive equation formulation.

The simulated working regimes were performed with the increased longitudinal advance. This fact was generated some non-uniformity on the smoothed surfaces.

The numerical simulation of the smooth finishing process was validated experimental on the special device. In Fig. 7 is shown the result of the experimental smooth finishing process, applied on the cylindrical workpieces. It is visible a new quality on the workpiece after processing.

The lamellar graphite in the material structure has a negative influence on the plastic deformation, by the quality limiting.

It has been established that a better smoothing by using a pressing force on the tool of 500 N is possible. It is found that on the machined surface, with some periodicity, corrugations occur. These corrugations varies in tight limits when is applied the force of 500 N. Largest corrugations occur when the push force increases.

Machining with forces greater than 1000 N, greatly reduces roughness but produces larger deviations form by corrugations.

The numerical simulation offers the large possibilities for design, analysis and optimizing of the working regimes for the smooth finishing processing.

The result of numerical simulation of the process of smoothing and hardening by displacement control is that the quality of the obtained surfaces is the best.

It can be considered that the numerical simulation of the process of smoothing and hardening by plastic deformation contributed greatly to the understanding and justification of the specific aspects of this technology.

7. ACKNOWLEDGEMENTS

We thank the teams of the University Polytechnic of Bucharest, National Research and Development Institute for Gas Turbines - COMOTI Bucharest, Technical University "Gheorghe Asachi" of Iasi for their support in conducting numerous tests carried out in several laboratories.

8. REFERENCES

► Khachanov, L.M. (1974). *Fundamentals of the Theory of the Plasticity*, Mir Publishers, Moscow

► Johnson, G.R., Cook W.H. (1983). *A constitutive Model and Data for Metals Subjected to Large Strains, High Strain Rates and High Temperatures*, Proceedings of Seventh International Symposium on Ballistics, Hague, pp. 541-547.

► Bathe, K.J. (1982). *Finite Element Procedures in Engineering Analysis*, Prentice-Hall.

► Bathe, K.J., Dvorkin, E.N. (1984). *A Continuum Mechanics Based Four-Node Shell Element for General Nonlinear Analysis*, Engineering computations, Vol. 1, No. 1, 77-88.

► Cook, R.D. (1974). *Concepts and Applications of Finite Element Analysis*, J. Wiley and Sons.

► Bathe, K.J., Wilson, E.L. (1976) *Numerical Methods in Finite Element Analysis*, Prentice-Hall.

9. NOTATION

$d\varepsilon_{ij}$= increments of plastic strain
s_{ij}= components of stress deviator
$d\lambda$= infinitesimal factor
σ_y= yielding stress
ε_p - effective plastic strain
A, B and n= material constants